Journal of Materials Chemistry C

Accepted Manuscript

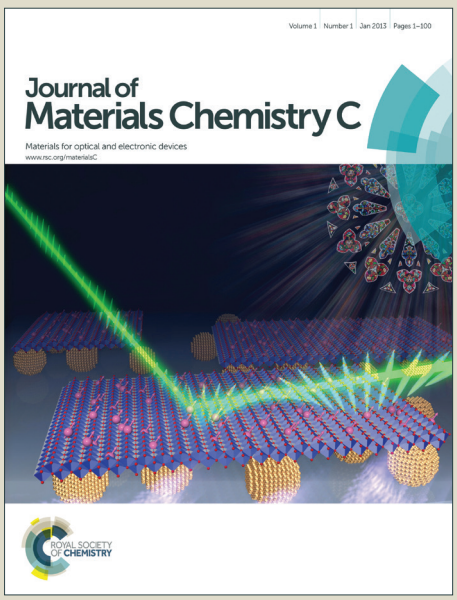

ROYAL SOCIETY OF CHEMISTRY

www.rsc.org/materialsC

Structure and Fluorescence Properties of Ternary Alumino Silicate Glasses doped with Samarium and Europium

Andreas Herrmann[1], Stefan Kuhn[1], Mirko Tiegel[1] and Christian Rüssel[1]

Jörg Körner[2], Diethard Klöpfel[2], Joachim Hein[2,3] and Malte C. Kaluza[2,3]

[1]Otto-Schott-Institut, Jena University, Fraunhoferstraße 6, 07743 Jena, Germany

[2]Institute of Optics and Quantum Electronics, Jena University, Max-Wien-Platz 1, 07743 Jena, Germany

[3]Helmholtz Institute Jena, Fröbelstieg 3, 07743 Jena, Germany

Abstract

Various ternary alumino silicate glasses with the molar compositions 20 Al_2O_3 – 60 SiO_2 – 20 R_2O (R = Li or Na), 20 Al_2O_3 – 60 SiO_2 – 20 RO (R = Mg, Ca or Zn) and 23.1 Al_2O_3 – 69.2 SiO_2 – 7.7 R_2O_3 (R = Y or La) doped with $1 \cdot 10^{20}$ Sm^{3+} cm^{-3} or $1 \cdot 10^{20}$ Eu^{3+} cm^{-3} (about 0.2 mol% Sm_2O_3/Eu_2O_3) were prepared. The glasses were studied with respect to their molecular structure, their thermo-mechanical and their fluorescence properties. All glasses show relatively broad fluorescence excitation and only a weak effect of the glass composition on the emission spectra is observed. Although the glasses should be structurally very similar, huge differences are found for the coefficients of thermal expansion and the glass transition temperatures. The fluorescence lifetime increases steadily with decreasing mean atomic weight and decreasing refractive index of the glasses, which may be explained by local field effects. The only exception from this rule is the zinc alumino silicate glass, which shows a relatively high fluorescence lifetime. The highest fluorescence lifetime is found for the lithium alumino silicate glass. The lowest coefficients of thermal expansion are found for zinc- and magnesium alumino silicate glasses. A low coefficient of thermal expansion is a prerequisite for a high thermal shock resistance of the material and hence favorable for high-power laser applications.

Introduction

Most glass-based laser amplifiers nowadays produced are realized using silica glass doped with ytterbium, neodymium or erbium oxides. The solubilities of these rare earth oxides in silica glass are comparably small, resulting in clustering of the rare earth ions at relatively low doping concentrations, which strongly decreases the fluorescence parameters such as the fluorescence lifetime of the dopants and the overall quantum efficiency. Therefore laser amplifiers based on silica glass are most commonly used in the form of optical fibers. Here the low rare earth doping concentrations can be compensated by increasing the interaction length i.e. the length of the fibers. Nevertheless, for ultra high-power laser applications, where laser pulses with peak powers of Terawatt or even Petawatt are generated, fiber amplifiers cannot be used since the necessary energy density and intensity in the comparatively small fiber core would exceed the destruction limit by many orders of magnitudes. Furthermore, non-linear effects such as self-phase modulation or self-focussing strongly deteriorate the temporal and spatial distribution of the light pulses which renders most high-power applications impossible[1]. Therefore, bulk glass amplifiers with larger rare earth oxide concentrations are necessary. This, however, cannot be achieved using pure SiO_2 as host material. Although the solubility of rare earth ions in silica glass can be substantially improved by aluminium codoping[2, 3], a large scale production of rare earth / Al_2O_3 co-doped SiO_2 bulk glass is very cost intensive due to the sophisticated production methods and very high melting temperature.

The amplifier materials used up to now in high-power bulk lasers are mostly ytterbium doped phosphate glasses[4], fluoride phosphate glasses[5, 6] or ytterbium doped calcium fluoride single crystals[7, 8]. The optical properties of these materials are exceptionally good, i.e. they show high fluorescence lifetimes and broad emission spectra[6, 9] enabling direct diode pumping and the amplification of sub-ps laser pulses. However, when used in amplification stages where Joule-class laser pulses are to be generated, micro cracks are likely to be formed in the glass, which increase light scattering and finally lead to a complete collapse of the laser operation or – after a further growth of these cracks – a destruction of the glass. The cause of this crack generation most likely is the high thermo-mechanical stress that is induced by the intense laser irradiation in conjunction with the high coefficients of thermal expansion, CTE, of these materials[10]. The latter are as large as $15 \cdot 10^{-6}$ K^{-1} for fluoride phosphate glasses[11] around $20 \cdot 10^{-6}$ K^{-1} for CaF_2[12] and larger than $12 \cdot 10^{-6}$ K^{-1} for phosphate glasses[4]. Furthermore the CTE strongly increases with increasing temperature.

Usually, the thermal shock behaviour of materials is described empirically using an appropriate figure-of-merit. In the literature, different figures-of-merit have been used (for a comparison see e.g. Hasselman[13]). In most of these formulae, the coefficient of thermal expansion is part of the denominator, while the thermal conductivity and the mechanical strength are part of the numerator.

Many boro silicate as well as alumino silicate glasses show comparatively small coefficients of thermal expansion[14, 15, 16] and also high Young's moduli and somewhat higher mechanical strengths than phosphate and fluoride phosphate glasses. In certain composition ranges, however, phase separation might occur. Alumino silicate glasses are widely used as glasses with good mechanical and good thermo-mechanical properties. Especially the $CaO/MgO/Al_2O_3/SiO_2$ system is well studied and is e. g. used for high modulus technical fibers which are used for polymer matrix composites. Glasses in the $MgO/(ZnO)/Al_2O_3/SiO_2$ system are used for glass-ceramics with excellent mechanical properties which are e. g. suitable as hard disc substrates[17] or as materials in dentistry[18]. Magnesium and zinc alumino silicates have good glass forming abilities[14, 15], high tensile strengths, high Young's moduli and especially low coefficients of thermal expansion[19]. In addition, alumino silicate glasses have a high chemical durability, a high solubility for rare earth oxides as well as comparably low OH solubility[20, 21]. Thus, alumino silicate glasses are promising candidates as laser host material, especially with respect to high-power laser applications. Nevertheless, in the literature the only alumino silicate glass frequently described as potential laser host material is the $La_2O_3/Al_2O_3/SiO_2$ system[22] and references therein.

In this article the effect of the glass composition on the structural, thermo-mechanical and fluorescence properties of rare earth-doped alumino silicate glasses is described. Li_2O, Na_2O, MgO, ZnO, CaO, Y_2O_3 and La_2O_3 have been used as network modifiers. Sm^{3+} or Eu^{3+} have been used as probing ion since the fluorescence lifetime of Yb^{3+} is difficult to measure because of strong reabsorption effects.

Experimental procedures

The glasses were prepared from high purity raw materials (Fe < 10 ppm, other contaminating metals < 0.5 ppm) SiO_2 (Sipur A1, Schott, Germany), Al_2O_3 (Ceralox, Condea Chemie, Germany), MgO (Merck, Germany), ZnO (Merck, Germany), $CaCO_3$ (Merck, Germany), Na_2CO_3 (Merck, Germany), Li_2CO_3

(Chemapol, Czech Republic), Y_2O_3 (Sigma-Alrich, Germany), $La_2O_3 \cdot H_2O$ (Laborchemie Apolda, Germany), Sm_2O_3 (Ferak, Germany) and Eu_2O_3 (Ferak, Germany). Batches of 100 to 200 g were melted in covered platinum crucibles at temperatures in the range from 1600 to 1650°C depending on the individual glass composition. Special measures for additional homogenization of the melts have not been applied. After melting for at least 3 hours, the samples were cast into preheated steel moulds and transferred into a muffle furnace, preheated to temperatures in the range from 720 to 920°C depending on T_g of the glass. Subsequently the cooling furnace was switched off and the samples were allowed to cool down (cooling rate: approximately 3 K/min).

Table 1 summarizes the chemical compositions of all prepared glasses. The samples were denoted according to their molar chemical composition. Most glasses were doped with samarium using samarium oxide as an additive to the raw materials. Some of the glasses were also prepared with europium doping. The doping concentration of Sm^{3+} or Eu^{3+} was kept constant at $1 \cdot 10^{20}$ ions per cm³ for all glass compositions which corresponds to about 0.2 mol% Sm_2O_3 or Eu_2O_3 depending on the density of the glass.

The glass transition temperatures T_g and the coefficients of thermal expansion CTE were measured using a dilatometer (DIL 402 PC, NETZSCH Gerätebau GmbH, Germany). For that purpose, cylindrical samples with a diameter of 8 mm and a length of about 20 mm had been prepared. The temperature range was 20 to 1000 °C and the heating rate 5 K/min. The densities were measured using a helium pycnometer (AccuPyc 1330, Micromeritics GmbH, Germany).

Fluorescence emission spectra were measured using a fluorescence spectrometer (RF-5301PC, SHIMADZU Japan); the samples were polished and had a thickness of 10 mm. Samarium excitation spectra were recorded at an emission wavelength of about 600 nm (615 nm for Eu^{3+}) while emission spectra were obtained using an excitation wavelength of about 400 nm (395 nm for Eu^{3+}) (spectral resolution: 0.2 nm). Fluorescence lifetimes were measured using a home-made experimental setup. For excitation of the glass samples a high intensity pulsed InGaN-diode (LED 395-66-60-110, Roithner Lasertechnik GmbH, Austria) with an emission wavelength of 395 nm was used. The emitted fluorescence light was collected and focused by a lens array onto the entrance slit of a monochromator (H.25, HORIBA Jobin Yvon, France). The spectrum-sliced light is amplified by a photomultiplier tube (R5929, Hamamatsu Photonics K.K., Japan) connected to a digital storage oscilloscope (TDS2012, TEKTRONIX USA). This setup allows for wavelength specific lifetime

measurements. Fluorescence lifetimes were measured for the strongest fluorescence transitions ($^4G_{5/2} \rightarrow {}^6H_{7/2}$ of Sm^{3+} at around 600 nm and $^5D_0 \rightarrow {}^7F_2$ of Eu^{3+} at around 615 nm).

Furthermore, Fourier-transformed IR (FTIR) spectra of all samples were recorded using a spectrometer (IRAFFINITY-1, Shimadzu Corp., Japan) with specular reflectance accessory (SRM-8000A). Reflection spectra were measured on polished glass samples in the wave number range from 400 to 2,000 cm^{-1}; subsequently the Kramers-Kronig-transformation was applied.

Results and discussion

In Table 1, the as weighted glass compositions are shown. For alkali- and earth alkali alumino silicate glasses the molar composition is 20% network modifier oxide, 20% Al_2O_3 and 60% SiO_2. The samples are named RAS2020 while R stands for the network modifier ion. To ensure the same network structure of all investigated glasses, those glasses containing Y_2O_3 and La_2O_3 have additionally been prepared with only 6.67 mol% Y_2O_3 and La_2O_3, while keeping the Al_2O_3 / SiO_2 ratio constant at 1:3. The normalized molar composition of these glasses is 7.7mol% Y_2O_3/La_2O_3, 23.1 mol% Al_2O_3 and 69.2 mol% SiO_2. These samples are named YAS0823 and LaAS0823 respectively. All prepared glass samples were visually transparent and homogeneous. Furthermore, Table 1 summarizes the glass transition temperatures, T_g, the refractive indices, n_e, the coefficients of linear thermal expansion, CTE, and the densities of all glass compositions. As expected, the density and the refractive index of the glasses increase with increasing atomic weight of the network modifier ion. For laser applications, a high refractive index is likely to be disadvantageous because of increased second order effects[23] which might lead to self focusing and self-phase modulation which strongly deteriorate the temporal and spatial characteristics of the pulses[24]. The lowest CTE of all investigated glasses are found for the magnesium and the zinc alumino silicate glasses (4.06 and $3.64 \cdot 10^{-6}$ K^{-1}, respectively). The highest CTE are found for the lithium- and sodium alumino silicate glasses. Low CTE are a prerequisite for a high resistance to thermo-mechanical shock. Glasses of low atomic weight, on the other hand, in general show relatively high thermal conductivity values if glasses of similar structure are discussed[25]. A high thermal conductivity should decrease the thermal stress of the material and therefore is beneficial for high power laser applications. Thermal conductivity is also increased by increasing network connectivity[25], but for most glasses investigated here, network connectivity should not change

much. For that reason thermal conductivity should be similar for most glass compositions that are discussed here. However, there should be a tendency to lower thermal conductivity for glasses of higher atomic weight.

Huge differences were found for the glass transition temperatures. In general, the glass transition temperatures are very high and lie in the range of 693 to 863 °C. The lowest T_g was found for lithium- and zinc-alumino silicate glasses. This might be advantageous for the glass production because lower melting temperatures are possible. Hence better homogenization of the glasses might be facilitated due to lower viscosities.

The FTIR absorption spectra of all investigated alumino silicate glasses are shown in Fig. 1. Basically, the spectra can be divided into 3 parts: the high energy part with wavenumbers above 850 cm^{-1}, the low energy part below 600 cm^{-1} and the part of medium energy in between (600 to 850 cm^{-1}).

The high energy part of all spectra is dominated by a high intensity, broad band in the range from 850 to 1250 cm^{-1}. The main peak of this band is located between 1050 and 1200 cm^{-1} and can be attributed to vibrations of two types of oxygen bridges, Si-O-Si and Si-O-Al [26]. According to Lee and Deventer[27] two asymmetric stretching bands due to Si-O-(Si, Al) units are observed at around 1115-1140 and 1080 cm^{-1}. Additionally, another band occurs at around 1165 cm^{-1} due to asymmetric stretching of Si-O-Si units. These bands reflect the “bridging” oxygen atoms (BO) that form the interlinkage of one $[SiO_4]$ group with another $[SiO_4]$ tetrahedron, as well as of a $[SiO_4]$ tetrahedron with an $[AlO_4]^-$ group. All these $[SiO_4]$ and $[AlO_4]^-$ tetrahedra form the glass network in alumino silicate glasses. For the occurrence of aluminum in fourfold coordination, i.e. as $[AlO_4]^-$ tetrahedra, the compensation of the negative charge is required. This can be achieved by the addition of appropriate quantities of network modifier oxides. Larger concentrations of network modifying oxides can also result in the splitting up of the bridging oxygen Si-O-(Si, Al) bonds and hence in the formation of non-bridging oxygen (NBO). In the IR spectra, the stretching vibration of these terminating $Si\text{-}O^-$ groups is attributed to the peak at around 950 cm^{-1} [26]. Hence, the intensity of this peak directly reflects the breaking of the network forming Si-O-(Si, Al) bonds. Furthermore, the formation of NBO sites also affects the position of the BO peak. The vibrational energy of $[SiO_4]$ tetrahedra coordinated with four bridging oxygen atoms is higher than those of $[SiO_4]$ groups coordinated with two or three bridging

oxygen atoms. Hence, a decreasing network connectivity results in the shift of the BO peak to smaller wavenumbers and therefore in a decrease of the maximum phonon energy[22]. For zinc- and magnesium alumino silicate glasses, the BO peak can be found at around 1150 cm^{-1} (Fig. 1). It is well separated from the NBO peak at around 950 cm^{-1}. For most other glasses, the BO peak is shifted to lower energies and the NBO peak can only be observed as a shoulder of the broadened BO peak.

In the medium energy range of the spectra in Fig. 1 between 600 and 850 cm^{-1}, mainly symmetric Si-O-(Si, Al) stretching modes are observed. As reported for vitreous silica, the symmetric stretching vibrations of Si-O-Si can be found at around 800 cm^{-1} [28]. In calcium alumino silicate glasses these vibrations are observed at wave numbers between 770 and 833 cm^{-1} [29]. In rare earth and cerium alumino silicate glasses the band is reported to occur at 780 cm^{-1} [30] and at 773 to 792 cm^{-1} [31], respectively. These data fit very well to our observations (see Fig. 1). The Al-O stretching vibrations are observed between 650 and 750 cm^{-1} [30]. Tarte found that vibrations in the range from 900 to 700 cm^{-1} can be attributed to "condensed" $[AlO_4]^-$ tetrahedra in crystalline materials[32]. "Isolated" $[AlO_4]^-$ tetrahedra absorb between 800 and 650 cm^{-1}. However, the spectra in Fig. 1 show a broad but mostly very weak band in this wavenumber range. But Al^{3+} ions can also act as network modifiers. In this case $[AlO_6]^{3-}$ octahedra are formed instead of $[AlO_4]^-$ tetrahedra. For "isolated" and "condensed" $[AlO_6]^{3-}$ octahedra the characteristic vibrational energies are reported to be at around 500 to 680 cm^{-1} and 400 to 530 cm^{-1} respectively[32]. Further, in the low energy part of the spectra in Fig. 1 below 600 cm^{-1} rocking vibrations of Si-O-Si and Si-O-Al units are found[26]. These dominate this wavenumber range. In charge compensated alumino silicate glasses, that means at network modifier oxide to aluminium oxide ratios of about 1, most of the Al^{3+} ions are found in $[AlO_4]^-$ tetrahedra. Shelby estimates the amount of Al^{3+} ions in $[AlO_6]^{3-}$ octahedra to be less than 10% in such glasses[33]. However, within this wavenumber range all spectra in Fig. 1 show approximately the same shape, and almost no variation between glasses of different composition is found.

The fluorescence excitation and emission spectra of three samarium doped glass types are shown in Figures 2 and 3, respectively. For comparison only the lithium-, calcium- and lanthanum alumino silicate glasses are displayed. All spectra are normalized to their most intense peaks at around 400 nm (excitation) and 600 nm (emission). Furthermore the different spectra are shifted in vertical direction for clarity. Relatively narrow bands attributed to the f-f-transitions of Sm^{3+} are observed, which are broadened in comparison to the transitions observed in crystals due to the irregular glass

structure and the attributed variation in the local sites of the Sm^{3+} ions. In the excitation spectra (Fig. 2) several small and one relatively intense excitation band are present. This intense excitation band is due to the transition $^6H_{5/2}$ (ground state) to $^6P_{3/2}$ at around 402 nm[34]. In general the excitation spectra of all glasses do not show notable differences. Only for the zinc alumino silicate glass (ZnAS2020), which is additionally shown in Fig. 2, a decrease in intensity for the transitions below 400 nm is observed in comparison to all other glasses. This effect is due to the broad absorption band of the zinc ions in glasses between 200 and 400 nm, which hinders the excitation of the Sm^{3+} ions in this wavelength range[35, 36].

Figure 3 shows the typical four fluorescence emission lines of the Sm^{3+} ion. The most intense line at around 600 nm is attributed to the transition $^4G_{5/2} \rightarrow {}^6H_{7/2}$. At 563, 646 and 705 nm, the transitions $^4G_{5/2} \rightarrow {}^6H_{5/2}$, $^4G_{5/2} \rightarrow {}^6H_{9/2}$ and $^4G_{5/2} \rightarrow {}^6H_{11/2}$ are respectively observed[34, 37]. The line shapes are hardly affected by compositional variations. A slight but steady shift in the emission spectra to longer wavelengths can be observed with lower atomic weight of the network modifying ion: e.g. the highest fluorescence emission peak of LaAS0823 is located at 598 nm while it is observed at 600 nm for the LiAS2020 glass.

Figure 4 shows the fluorescence decay curves of four Sm^{3+}-doped glass types. After excitation at 395 nm by the high-power LED, fluorescence rises quickly to its maximum value (not shown), which is kept for several milliseconds (normalised fluorescence intensity level at $t<0$). At $t=0$, the diode is switched off and the fluorescence intensity of the samples drops with distinct characteristics. Due to the half-logarithmic scale, a mono-exponential decay appears as a straight line. The slope of this line corresponds to the inverse fluorescence lifetime. For all samples an almost mono exponential decay is observed, which indicates an almost undisturbed fluorescence emission process and homogeneously distributed fluorophores. The slight deviations from mono exponential decays most likely are due to cross-relaxation processes. For clarity only 4 decay curves are displayed in Fig. 4. The lifetimes vary between 2.2 ms (lanthanum alumino silicate) and 2.7 ms (lithium alumino silicate). The fluorescence lifetimes of all glasses are included in Table 1. The fluorescence lifetime decreases steadily with increasing atomic weight of the network modifier ions and therefore also with increasing refractive index of the glasses. The only exception from this rule is, again, the zinc alumino silicate sample. Its relatively long fluorescence lifetime is only surpassed by the lithium alumino silicate glass. In general, the same behaviour is also found for Sm^{3+}-doped ternary alumino silicate glasses of the molar

composition 15/15/70 (Table 1). Even lower fluorescence lifetimes were found for glasses with higher lanthanum concentration[22] and tantalum containing alumino silicate glasses (not shown). According to frequent reports in the literature, the fluorescence lifetime should increase with decreasing phonon energies of the glass network. Hence, it should be assumed, that those compositions which show low phonon energies should also show high fluorescence lifetimes. Although figure 1 suggests a slightly lower phonon energy for lithium and sodium alumino silicate glasses in comparison to the other glasses depicted in this figure (peak position and high energy offset of the peak at around 900 to 1300 cm^{-1}), previous detailed studies of magnesium and lanthanum alumino silicate glasses, however, found no correlation between phonon energy and fluorescence lifetime in Sm^{3+}-doped alumino silicate glasses[22, 38]. For both glass systems the maximum phonon energy could be reduced by increasing the network modifier concentrations. This resulted in a decrease of the fluorescence lifetime in lanthanum alumino silicate glasses while it did not show a significant effect for the magnesium alumino silicate glasses. A clear correlation to other parameters of the network modifying ions such as electronegativity, ionic radius or ionization energy can also be ruled out easily by comparing the tabulated data with the measured fluorescence lifetimes. A clear dependency upon the optical basicity of the glass host can also be ruled out, although a general trend to higher lifetimes for low basicity glasses can be observed. Furthermore the OH^- concentrations of all glasses have been measured using IR-spectroscopy (Table 1). In the wavenumber range between 3000 and 3700 cm^{-1} all glasses show low E/d (extinction/thickness) values between 1.4 and 0.4 cm^{-1} which correspond to OH^- concentrations between 1.3 and $0.4 \cdot 10^{19}$ cm^{-3} assuming OH^- extinction coefficients to be the same as for soda lime silica glasses[21, 38]. The shape of the OH^- absorption band (particularly the high energy offset of the band) also doesn't change for all glasses. A correlation between OH^- concentration and fluorescence lifetime in this concentration range was not found (Table 1). Hehlen et al. show that OH^- concentrations in this range have only little influence on the quantum efficiency (and therefore on the fluoerescence lifetime) of the $^4I_{13/2}$ level of Er^{3+} in alumino silicate glasses at relatively low rare earth doping concentrations of around 0.2 mol% [39]. The $^4G_{5/2}$ emission of Sm^{3+} should be even less influenced than the $^4I_{13/2}$ emission of Er^{3+} because of the bigger energy gap to the next lower energy level (around 7,400 cm^{-1} and 6,500 cm^{-1} respectively[34]). However, all these parameters, especially the ion radius of the network modifier ions and OH^- concentration might have a minor effect on the fluorescence lifetime of the doped rare earth elements. A clear correlation was found for the mean atomic weight of the glass composition and therefore for the mean atomic number of the network

modifier ion if glasses of constant molar fractions of the glass components are compared (e. g. 20/20/60). Figure 5 shows the dependency of the Sm^{3+} fluorescence lifetime on the mean atomic weight of ternary alumino silicate glasses. Data points of the glasses reported here are filled, while the additional data (not filled data points) is taken from earlier publications[22, 38] and some glasses with a somewhat different molar composition. The systematical error of the lifetime measurements due to sample preparation and experimental setup can be estimated to less than 2%. The biggest uncertainty is due to cross-relaxation processes and OH^- quenching. While cross-relaxation processes mainly depend on the Sm^{3+} doping concentration which is kept constant and therefore has a consistent influence on all samples, OH^- quenching in this OH^- concentration range causes an error of about 10% [39]. To be able to estimate the influence of OH^- quenching on the measurement, the size of the filled circles represents the OH^- concentration of the specific glass sample. But despite all disturbance, an almost linear dependence of the fluorescence lifetime on the mean atomic weight of the glass composition can be observed. The same dependency was found for Eu^{3+}-doped alumino silicate glasses which were additionally prepared. These data points (triangles) are also added to the diagram. While the Sm^{3+} measurements might be slightly influenced by OH^- quenching as discussed above, the $^5D_0$ emission of Eu^{3+} should be almost free of any OH^- quenching because of the huge energy gap of around 12,000 cm^{-1} [45]. This can be shown easily by applying the so called energy-gap law[39]. Also, cross-relaxation processes do not occur for Eu^{3+}-doped materials in this concentration range[46].

According to Bardez et al., rare earth ions (Nd^{3+} in this case) enter depolymerized regions of the glass matrix (sodium calcium alumino silicate system in this case)[40]. It was shown by extended X-ray absorption fine structure (EXAFS) measurements, that sodium and calcium ions are likely to be present in the second coordination shell of the Nd^{3+} ions. A similar behavior of rare earth ions (Er^{3+} and Eu^{3+}) is reported by Du, Cormack and Kokou for binary alkali silicate glasses[41, 42]. A very nice depiction of such depolymerized regions in alkali silicate glasses can be found in Ref. [43]. This behavior of rare earth ions could well explain the strong dependence of the fluorescence lifetime on the network modifier, assuming that closely coordinated network modifying ions have a substantial influence on the parameters of the rare earth sites as e.g. crystal field strength and symmetry. Unfortunately, the spectra of the Sm^{3+}-doped glasses presented in figures 2 and 3 do not show notable variations with the glass composition. For this reason, few Eu^{3+}-doped glasses have additionally been prepared since Eu^{3+} has a hypersensitive transition which is strongly dependent on the local symmetry at the rare earth site[37, 44]. Figure 6 shows fluorescence emission spectra of two Eu^{3+}-doped glasses, a lithium and

a lanthanum alumino silicate glass. Note that the two spectra are shifted vertically for clarity. For excitation, a wavelength of 395 nm was used. Both spectra are normalized to the strongest fluorescence emission line at about 615 nm which is assigned to the transition $^5D_0 \rightarrow {}^7F_2$ [45]. This transition is almost entirely electric dipole in nature and therefore sensitive to the local crystal field symmetry[44]. The other peaks are assigned to the transitions $^5D_0 \rightarrow {}^7F_0$ at about 575 nm, $^5D_0 \rightarrow {}^7F_1$ at about 590 nm, $^5D_0 \rightarrow {}^7F_3$ at about 655 nm and $^5D_0 \rightarrow {}^7F_4$ at about 700 nm[45]. The transitions at 575 and 590 nm can hardly be distinguished because of the strong splitting of the 590 nm line. The latter of these two ($^5D_0 \rightarrow {}^7F_1$ at 590 nm) is an almost pure magnetic dipole transition which is not influenced by local site symmetry[44]. Therefore the intensity ratio of the emission peaks at 590 and 615 nm, I_{590}/I_{615}, can be used as measure for the overall symmetry at the local Eu^{3+} site. A high ratio I_{590}/I_{615} indicates a high crystal field symmetry and vice versa[44]. Unfortunately, a clear differentiation between the intensity ratios of the peaks in the two spectra of figure 6 is not possible, although the peak at 590 nm in lanthanum alumino silicate is slightly higher than in lithium alumino silicate which should indicate a slightly higher symmetry in the lanthanum containing glass[37, 44]. Nevertheless, because of the relatively low intensity ratio I_{590}/I_{615} of both glasses (see Figure 6), it can be stated that the rare earth site symmetry in alumino silicate glasses is generally very low. This is not surprising since similar observations have been made for other silicate glasses[46]. In contrast to alumino silicate glasses, fluoride based glasses offer a much higher symmetry at the local Eu^{3+} sites. Here, much higher intensity ratios I_{590}/I_{615} were found[46]. In summary, a clear estimation of individual symmetry or crystal field strength cannot be made for the glasses investigated here. However, Brecher and Riseberg as well as Lochhead and Bray found decreasing fluorescence lifetimes for Eu^{3+} ions at sites with locally increased crystal field by laser-induced fluorescence line narrowing (LFLN) measurements[47, 48]. On the other hand it is well known, that spontaneous emission can be changed by altering the refractive index of the surrounding dielectric media. Since the first publication of this effect by Purcell[49] many theoretical e. g. [50-54] and experimental e. g. [54] and references therein studies have been published on this topic, although only few of the experimental work has been done on glasses so far [55-57]. Among the various theoretical models that predict the dependence of the spontaneous emission rates A^{diel} on the refractive index n of the surrounding dielectric medium are the real-cavity[58] and the virtual-cavity model[59]. In general this dependency can be written as: $A^{diel}(n) = n \cdot l(n)^2 \cdot A_0$. Here, A_0 is the vacuum spontaneous emission rate and l is the dielectric local-field correction factor which differs for the various models. For the real-cavity model it is defined as $l(n) = 3n^2/(2n^2 + 1)$ [58] and for the virtual-cavity

model $l(n) = (n^2 + 2)/3$ [59]. Since $n \geq 1$ the spontaneous emission rate is increased (and the lifetime of the excited state is decreased) by the dielectric medium around the emitter with increasing n, and accordingly with increasing interaction of the emitter and the surrounding dielectric medium. Figure 7 shows the fluorescence lifetimes of Sm^{3+}-doped glasses in dependence of the measured refractive index n_e of the samples together with the least-square fit of both models. Although both models represent the experimental data about right it is difficult to decide which one fits the data better. As discussed earlier, the fluorescence lifetime of the Sm^{3+}-doped samples is additionally influenced by various effects, most notably OH^- quenching and cross-relaxation processes (slight deviation from mono-exponential fluorescence decay in Fig. 4 [60]) which distort the relation between fluorescence lifetime and refractive index for the measurements presented here. Furthermore, the observed fluorescence transition of Sm^{3+} ($^4G_{5/2} \rightarrow {}^6H_{7/2}$) has a notable magnetic dipole contribution and therefore is not entirely electric dipole dominated[61] which is required to apply the two models. Magnetic dipole transitions show a different dependence on the refractive index of the surrounding medium[50]. In analogy to the Sm^{3+}-doped glasses, Fig. 8 shows the fluorescence lifetimes of the Eu^{3+}-doped samples in dependence of the measured refractive indices. Again, the virtual and real cavity model have been fitted to the data. Here, the real cavity model reproduces the data much better than the virtual cavity model, although the data consists of only 4 samples. Nevertheless, this result is in agreement with previous studies on glasses[55, 56]. In contrast to Sm^{3+}, the measured transition of Eu^{3+} ($^5D_0 \rightarrow {}^7F_2$) is much less sensitive to cross-relaxation processes and OH^- quenching[46]. Furthermore, it has an almost entirely electric dipole character[44].

However, also the theoretical models are based on the variation of the inhomogeneous, time-dependent electromagnetic local field around the emitting atom. Hence, the observations of Brecher and Riseberg as well as Lochhead and Bray[47, 48] are not in disagreement with the theoretically derived refractive index-dependency since the average effective field strength is correlated to the density of the surrounding atoms which form the dielectric medium[53].

Besides their advantageous properties, such as high solubility for rare earth ions, broad excitation and emission spectra of doped rare earth ions, good glass forming ability, low coefficients of thermal expansion and high mechanical strengths, alumino silicate glasses can also provide relatively long fluorescence lifetimes. Obviously network modifying ions of low atomic weight as well as Zn^{2+} can substantially improve the fluorescence lifetime of doped rare earth ions in this glass system.

Conclusions

Alumino silicate glasses with the molar compositions 20 Al_2O_3 – 60 SiO_2 – 20 R_2O (R = Li or Na), 20 Al_2O_3 – 60 SiO_2 – 20 RO (R = Mg, Ca or Zn) and 20 Al_2O_3 – 73.33 SiO_2 – 6.67 R_2O_3 (R = Y or La) doped with $1 \cdot 10^{20}$ Sm^{3+} cm^{-3} or $1 \cdot 10^{20}$ Eu^{3+} cm^{-3} (about 0.2 mol% Sm_2O_3/Eu_2O_3) were prepared and investigated with respect to their molecular structure and their thermo-mechanical as well as optical properties. The glasses show broad fluorescence excitation and emission spectra that are hardly affected by the glass composition which is a mandatory requirement for chirped pulse laser amplification. Although the glasses should be structurally very similar, significant differences are found for the coefficients of thermal expansion, the glass transition temperatures and the fluorescence lifetimes. The fluorescence lifetime increases steadily with decreasing atomic weight and decreasing refractive index of the glasses. The only exception from this rule is the zinc alumino silicate glass which shows a longer fluorescence lifetime than the calcium- and magnesium alumino silicate glasses. Its relatively long fluorescence lifetime is only surpassed by the lithium alumino silicate glass. The zinc alumino silicate glass also provides one of the lowest glass transition temperatures which should be beneficial for the production and the optical quality of the glass. Furthermore, it shows the lowest coefficient of thermal expansion of all investigated glasses which is highly advantageous for a high thermal shock resistance. Hence, a zinc alumino silicate glass could be a promising laser material especially with respect to ultra high-power systems or applications with high repetition rates.

Acknowledgments

This work was supported by the European Social Fund (ESF) through the Thuringian Ministry of Economy, Employment and Technology (project number 2011 FGR 0122).

Table 1: Molar compositions, transition temperatures T_g, density, refractive index n_e, coefficients of thermal expansion CTE, fluorescence lifetimes ($1 \cdot 10^{20}$ Sm^{3+} cm^{-3}) and OH^- absorption coefficients of homogeneous glass samples.

sample name	composition (mol%)			T_g	density	n_e	CTE	τ_{Sm3+}	E_{OH}/d
				(°C)	(g/cm^3)		(10^{-6} K^{-1})	(ms)	(cm^{-1})
	M_2O / MO / M_2O_3	Al_2O_3	SiO_2	± 3	± 0.005	± 0.005	± 0.1	± 0.03	± 0.05
LiAS2020	Li_2O: 20	20	60	693	2.40	1.531	7.64	2.65	1.27
LiAS1515	Li_2O: 15	15	70	820	2.36	1.521	6.64	2.62	1.06
NaAS2020	Na_2O: 20	20	60	811	2.45	1.507	9.46	2.45	1.37
NaAS1515	Na_2O: 15	15	70	813	2.38	-	7.98	2.56	1.17
MgAS2020	MgO: 20	20	60	827	2.55	1.548	4.06	2.43	0.73
MgAS1515	MgO: 15	15	70	831	2.44	1.520	3.22	2.47	0.37
CaAS2020	CaO: 20	20	60	868	2.61	1.557	5.71	2.37	1.00
CaAS1515	CaO: 15	15	70	876	2.50	-	5.05	2.51	0.85
ZnAS2020	ZnO: 20	20	60	742	2.84	1.573	3.64	2.51	0.99
ZnAS1515	ZnO: 15	15	70	757	2.68	-	3.10	2.47	0.83
YAS0823	Y_2O_3: 7.7	23.1	69.2	899	2.85	1.581	4.31	2.28	1.32
LaAS2020	La_2O_3: 20	20	60	863	4.08	1.709	6.50	2.01	0.76
LaAS1515	La_2O_3: 15	15	70	862	3.57	1.648	5.43	2.12	0.93
LaAS0823	La_2O_3: 7.7	23.1	69.2	875	3.02	1.593	4.43	2.23	0.85

References

1 J. Limpert, S. Hädrich, J. Rothhardt, M. Krebs, T. Eidam, T. Schreiber and A. Tünnermann, Ultrafast fiber lasers for strong-filed physics experiments. Laser & Photonics Reviews, 2011, 5, 634-646.

2 A. J. Kenyon, Recent developments in rare-earth doped materials for optoelectronics. Prog. Quantum Electron., 2002, 26, 225–284.

3 K. Arai, H. Namikawa, K. Kumata, T. Honda, Y. Ishii and T. Handa, Aluminum or phosphorus co-doping effects on the fluorescence and structural properties of neodymium-doped silica glass. J. Appl. Phys., 1986, 59, 3430-3436.

4 J. H. Campbell, J. S. Hayden and A. Marker, High-Power Solid-State Lasers: a Laser Glass Perspective. Int. J. Appl. Glass Sci., 2011, 2, 3-29.
DOI: 10.1111/j.2041-1294.2011.00044.x

5 J. Hein, S. Podleska, M. Siebold, M. Hellwing, R. Bödefeld, R. Sauerbrey, D. Ehrt and W. Wintzer, Diode-pumped chirped pulse amplification to the joule level, Appl. Phys. B: Lasers Opt., 2004, 79, 419-422.
DOI: 10.1007/s00340-004-1586-3

6 D. Ehrt, Fluoroaluminate glasses for lasers and amplifiers, Curr. Opin. Solid State Mater. Sci., 2003, 7, 135-141.

7 M. Siebold, M. Hornung, R. Bödefeld, S. Podleska, S. Klingebiel, C. Wandt, F. Krausz, S. Karsch, R. Ücker, A. Jochmann, J. Hein and M. C. Kaluza, Terawatt diode-pumped Yb:CaF2 laser, Opt. Lett., 2008, 33, 2770-2772.

DOI: 10.1364/OL.33.002770

8 J. Körner, C. Vorholt, H. Liebetrau, M. Kahle, D. Klöpfel, R. Seifert, J. Hein and M. C. Kaluza, Measurement of temperature-dependent absorption and emission spectra of Yb:YAG, Yb:LuAG, and Yb:CaF2 between 20 °C and 200 °C and predictions on their influence on laser performance, J. Opt. Soc. Am. B, 2012, 29, 2493-2502.

DOI: 10.1364/JOSAB.29.002493

9 M. Siebold, M. Hornung, S. Bock, J. Hein, M. C. Kaluza, J. Wemans and R. Uecker, Broad-band regenerative laser amplification in ytterbium-doped calcium fluoride (Yb:CaF2). Appl. Phys. B: Lasers Opt., 2007, 89, 543-547.

10 R. M. Wood, Laser-induced damage of optical materials, Institute of Physics Publishing: Bristol and Philadelphia, 2003

11 D. Möncke, D. Ehrt, L. L. Velli, C. P. E. Versamis and E. I. Kamitsos, Structure and properties of mixed phosphate and fluoride glasses. Phys. Chem. Glasses, 2005, 46, 67-71.

12 S. S. Ballard, S. E. Brown and J. S.Browder, Measurements of thermal-expansion of 6 optical-materials, from room-temperature to 250 degrees C. Appl. Opt., 1978, 17, 1152-1154.

DOI: 10.1364/AO.17.001152

13 D. P. H. Hasselman, Figures-of-merit for the thermal stress resistance of high-temperature brittle materials: a review. Ceram. Int., 1978, 4, 147-150.

14 S. M. Logvinkov, G. D. Semchenko and D. A. Kobyzeva, Rearrangement of conodes of the phase diagram of the MgO-Al2O3-SiO2 system and its technological prospects. Refractories, 1996, 37, 378-381.

15 D. Ehrt, H. T. Vu, A. Herrmann and G. Voelksch, Luminescent ZnO-Al2O3-SiO2 glasses and glass ceramics. Adv. Mater. Res., 2008, 39-40, 231-236.

DOI: 10.4028/www.scientific.net/AMR.39-40.231

16 D. Möncke, D. Ehrt, H. Eckert and V. Mertens, Influence of melting and annealing conditions on the structure of borosilicate glasses. Phys. Chem. Glasses, 2003, 44, 113-116.

17 A. Hunger, G. Carl, A. Gebhardt and C. Rüssel, Young's moduli and microhardness of glass–ceramics in the system MgO/Al2O3/TiO2/ZrO2/SiO2 containing quartz nanocrystals. Mater. Chem. Phys., 2010, 122, 502-506.

DOI: 10.1016/j.matchemphys.2010.03.034

18 M. Dittmer and C. Rüssel, Colorless and high strength MgO/Al2O3/SiO2 glass-ceramic dental material using zirconia as nucleating agent. J. Biomed. Mater. Res. Part B, 2012, 100B, 463-470.

DOI: 10.1002/jbm.b.31972

19 M. Dittmer, M. Müller and C. Rüssel, Self-organized nanocrystallinity in MgO–Al2O3–SiO2 glasses with ZrO2 as nucleating agent. Mater. Chem. Phys., 2010, 124, 1083-1088.

DOI: 10.1016/j.matchemphys.2010.08.037

20 G. Leturcq, G. Berger, T. Advocat, C. Fillet, C. Halgand and E. Vernaz, Chemical Durability of Aluminosilicate Glasses Containing Low Solubility Chemical Elements, MRS Proceedings, 1997, 506, 199.

DOI: 10.1557/PROC-506-199

21 H. Scholze, Glastechnische Berichte, 1959, 32, 142-152.

22 S. Kuhn, A. Herrmann, J. Hein, M. C. Kaluza and C. Rüssel, Sm3+-Doped La2O3-Al2O3-SiO2-Glasses – Structure, Fluorescence and Thermal Expansion. J. Mater. Sci., 2013, 48, 8014–8022.

DOI: 10.1007/s10853-013-7613-1

23 M. Sheik-Bahae and E.W. Van Stryland, Optical nonlinearities in the transparency region of bulk semiconductors. Nonlinear Optics in Semiconductors, 1999, 58, 257-318.

24 T. Töpfer, J. Hein, J. Philipps, D. Ehrt and R. Sauerbrey, Tailoring the nonlinear refractive index of fluoride-phosphate glasses for laser applications. Appl. Phys. B, 2000, 71, 203-206.

25 M. M. Ammar, S. Gharib, M. M. Halawa, Kh. El Badry, N. A. Ghoneim, H. A. El Batal, Thermal conductivity of some silicate glasses in relation to composition and structure. J. Non-Cryst. Solids., 1982, 53, 165-172.

DOI: 10.1016/0022-3093(82)90026-6

26 M. Handke, W. Mozgawa and M. Nocun, Specific features of the IR spectra of silicate glasses. J. Mol. Struct., 1994, 325, 129-136.

27 W. K. W. Lee and J. S. J. van Deventer, The use of infrared spectroscopy to study geopolymerization of heterogeneous amorphous aluminosilicates. Langmuir, 2003, 19, 8726–8734.

DOI: 10.1021/la026127e

28 A. Efimov, Quantitative IR spectroscopy: Applications to studying glass structure and properties. J. Non-Cryst. Solids., 1996, 203, 1-11.

DOI: 10.1016/0022-3093(96)00327-4

29 C. Huang and E. Behrman, Structure and properties of calcium aluminosilicate glasses. J. Non-Cryst. Solids., 1991, 128, 310-321.
DOI: 10.1016/0022-3093(91)90468-L

30 J. T. Kohli, R. A. Condrate and J. R. Shelby, Raman and infrared-spectra of rare earth aluminosilicate glasses. Phys Chem. Glasses, 1993, 34, 81-87.

31 S. Lin, C. Hwang and J. Lee, Characterization of CeO2-Al2O3-SiO2 glasses by infrared and x-ray absorption near edge structure spectroscopies. J. Mater. Res., 1996, 11, 2641-2650.

DOI: 10.1557/JMR.1996.0332

32 P. Tarte, Infra-red spectra of inorganic aluminates and characteristic vibrational frequencies of AlO4 tetrahedra and AlO6 octahedra. Spectrochim Acta, Part A, 1967, 23, 2127-2143.

DOI: 10.1016/0584-8539(67)80100-4

33 J. E. Shelby, J. Appl. Phys., 1978, 49, 5885-5891

DOI: 10.1063/1.324553

34 W. Carnall, P. Fields and K. J. Rajnak, Chem. Phys., 1968, 49, 4424-4442.

DOI: 10.1063/1.1669893

35 G. Qian, M. Nikl, J. Bei, J. Pejchal, S. Baccaro, R. Giorgi, A. Cecilia and G. Chen, Temperature dependence of photoluminescence in ZnO-containing glasses. Opt. Mater., 2007, 30, 91–94.

36 G. Chen, M. Nikl, N. Solovieva, A. Beitlerova, J. Rao, Y. Yang, Y. Zhang, X. Jiang and C. Zhu, Photoluminescent properties of nanocrystallized zinc borosilicate glasses. Radiat. Meas., 2004, 38, 771–774.

37 G. Blasse and B.C. Grabmaier, Luminescent Materials, Springer: Berlin and New York, 1994

38 M. Tiegel, A. Herrmann, C. Rüssel, J. Körner, D. Klöpfel, J. Hein and M. C. Kaluza, Magnesium aluminosilicate glasses as potential laser host material for ultrahigh power laser systems. J. Mater. Chem. C, 2013, 1, 5031-5039.

DOI: 10.1039/c3tc30761a

39 M. P. Hehlen, N. J. Cockroft, T. R. Gosnell, and A. J. Bruce, Spectroscopic properties of Er3+- and Yb3+-doped soda-lime silicate and aluminosilicate glasses. Phys. Rev. B, 1997, 56, 9302-9318.

40 I. Bardez, D. Caurant, P. Loiseau, N. Baffier, J. L. Dussossoy, C. Gervais, F. Ribot and D. R. Neuville, Structural characterisation of rare earth rich glasses for nuclear waste immobilisation. Phys. Chem. Glasses, 2005, 46, 320–329.

41 J. Du and A. N. Cormack, The structure of erbium doped sodium silicate glasses. J. of Non-Cryst. Solids, 2005, 351, 2263–2276.

DOI: 10.1016/j.jnoncrysol.2005.05.018

42 L. Kokou and J. Du, Rare earth ion clustering behavior in europium doped silicate glasses: Simulation size and glass structure effect. J. Non-Cryst. Solids, 2012, 358, 3408–3417.

DOI: 10.1016/j.jnoncrysol.2012.01.068

43 B. Vessal, G. N. Greaves, P. T. Marten, A. V. Chadwick, R. Mole and S. Houde-Walter, Cation microsegregation and ionic mobility in mixed alkali glasses. Nature, 1992, 356, 504-506

DOI: 10.1038/356504a0

44 F.S. Richardson, J. D. Saxe, S. A. Davis and T. R. Faulkner, Mol. Phys., 1981, 42, 1401-1429.

45 W. Carnall, P. Fields and K. J. Rajnak, Chem. Phys., 1968, 49, 4450-4455.

46 A. Herrmann, S. Fibikar and D. Ehrt, Time-resolved fluorescence measurements on Eu3+- and Eu2+-doped glasses. J. Non-Cryst. Solids, 2009, 355, 2093–2101.

47 C. Brecher and L. A. Riseberg, Laser-induced fluorescence line narrowing in Eu glass: A spectroscopic analysis of coordination structure. Phys. Rev. B, 1976, 13, 81-93.

48 M. J. Lochhead and K. L. Bray, High-pressure fluorescence line narrowing of Eu(III)-doped sodium disilicate glass. Phys. Rev. B, 1995, 52, 15763-15775.

49 E. M. Purcell, Spontaneous Emission Probabilities at Radio Frequencies. Phys. Rev., 1946, 69, 674-674.

DOI: 10.1103/PhysRev.69.674.2

50 R. J. Glauber and M. Lewenstein, Quantum optics of dielectric media. Phys. Rev. A, 1991, 43, 467-491.

51 P. de Vries and A. Lagendijk, Resonant Scattering and Spontaneous Emission in Dielectrics: Microscopic Derivation of Local-Field Effects. Phys. Rev. Lett., 1998, 81, 1381-1384.

52 M. E. Crenshaw and C.M. Bowden, Effects of Local Fields on Spontaneous Emission in Dielectric Media. Phys. Rev. Lett., 2000, 85, 1851-1854.

DOI: 10.1103/PhysRevLett.85.1851

53 P. R. Berman and P. W. Milonni, Microscopic theory of modified spontaneous emission in a dielectric. Phys. Rev. Lett., 2004, 92, 0536011-0536014.

DOI: 10.1103/PhysRevLett.92.053601

54 M. E. Crenshaw, The quantized field in a dielectric and application to the radiative decay of an embedded atom. Phys. Lett. A, 2006, 358, 438–442.

DOI: 10.1016/j.physleta.2006.05.049

55 C.-K. Duan, M. F. Reid and Z. Wang, Local field effects on the radiative lifetime of emitters in sourrounding media: Virtual- or real-cavity model?. Phys. Lett. A, 2005, 343, 474-480.

DOI: 10.1016/j.physleta.2005.06.037

56 G. M. Kumar, D. N. Rao and G. S. Agarwal, Measurement of Local Field Effects of the Host on the Lifetimes of Embedded Emitters. Phys. Rev. Lett., 2003, 91, 2039031-2039034.

DOI: 10.1103/PhysRevLett.91.203903

57 C.-K. Duan, H. Wen and P. A. Tanner, Local-field effect on the spontaneous radiative emission rate. Phys. Rev. B, 2011, 83, 2451231-2451235.

DOI: 10.1103/PhysRevB.83.245123

58 D. Toptygin, Effects of the Solvent Refractive Index and Its Dispersion on the Radiative Decay Rate and Extinction Coefficient of a Fluorescent Solute. J. Fluoresc., 2003, 13, 201-219.

59 M. Born and E. Wolf, Principles of Optics., Cambridge University Press, Cambridge, 1999

60 A. Herrmann and D. Ehrt, Time-resolved fluorescence measurements on Dy3+ and Sm3+ doped glasses. J. Non-Cryst. Solids, 2008, 354, 916–926.

61 P. S. May, D. H. Metcalf, F. S. Richardson, R. C. Carter, C. E. Miller and R. A. Palmer, Measurement and analysis of excited-state decay kinetics and chiroptical activity in the 6Hj ← 4G5/2 transitions of Sm3+ in trigonal Na3[Sm(C4H4O5)3] · 2NaClO4 · 6H2O. J. Lumin., 1992, 51, 249-268.

DOI: 10.1016/0022-2313(92)90076-L

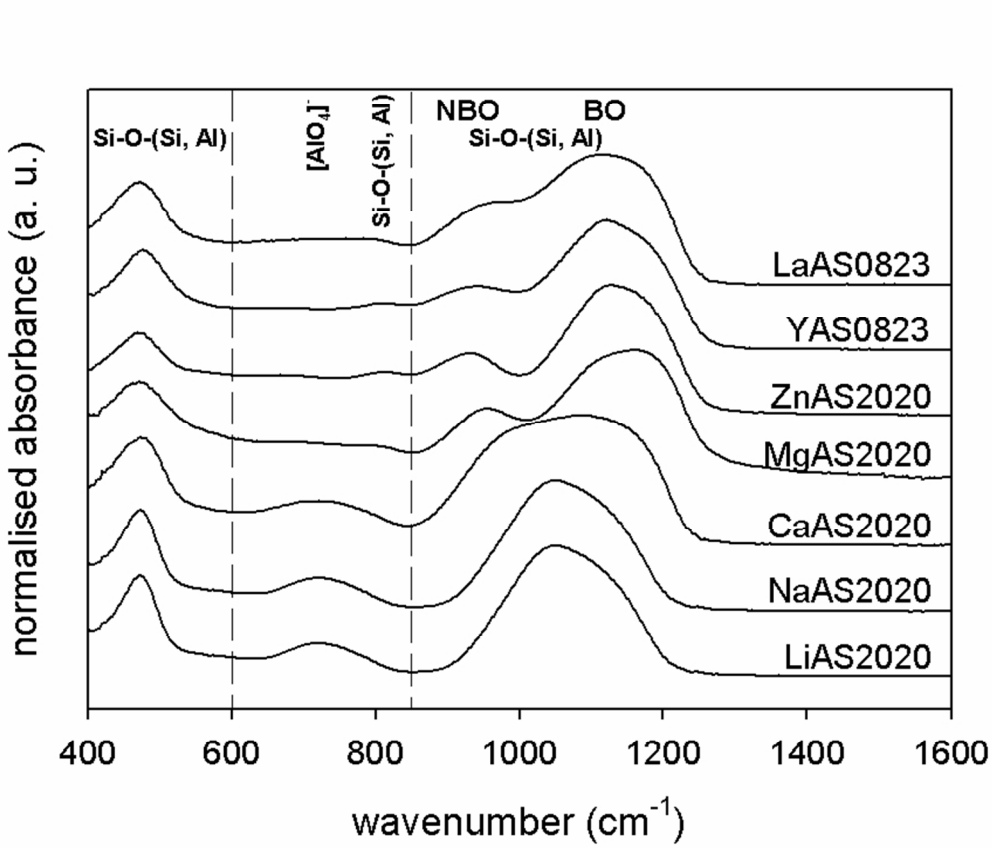

Fig. 1: FTIR absorbance spectra of different ternary alumino silicate glasses.
144x122mm (150 x 150 DPI)

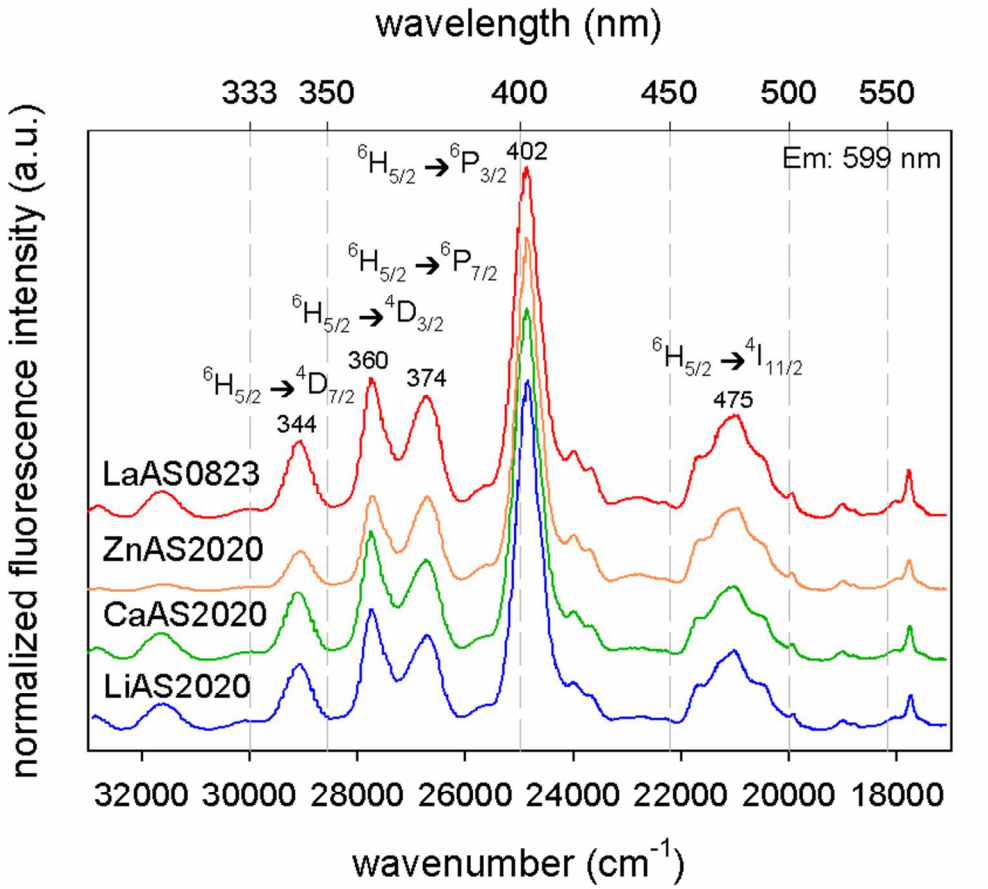

Fig. 2: Sm3+ excitation spectra of samples LiAS2020, CaAS2020, ZnAS2020 and LaAS0823 doped with 1·1020 Sm3+/cm3. Note that the different spectra have been shifted in vertical direction for clarity.
144x129mm (150 x 150 DPI)

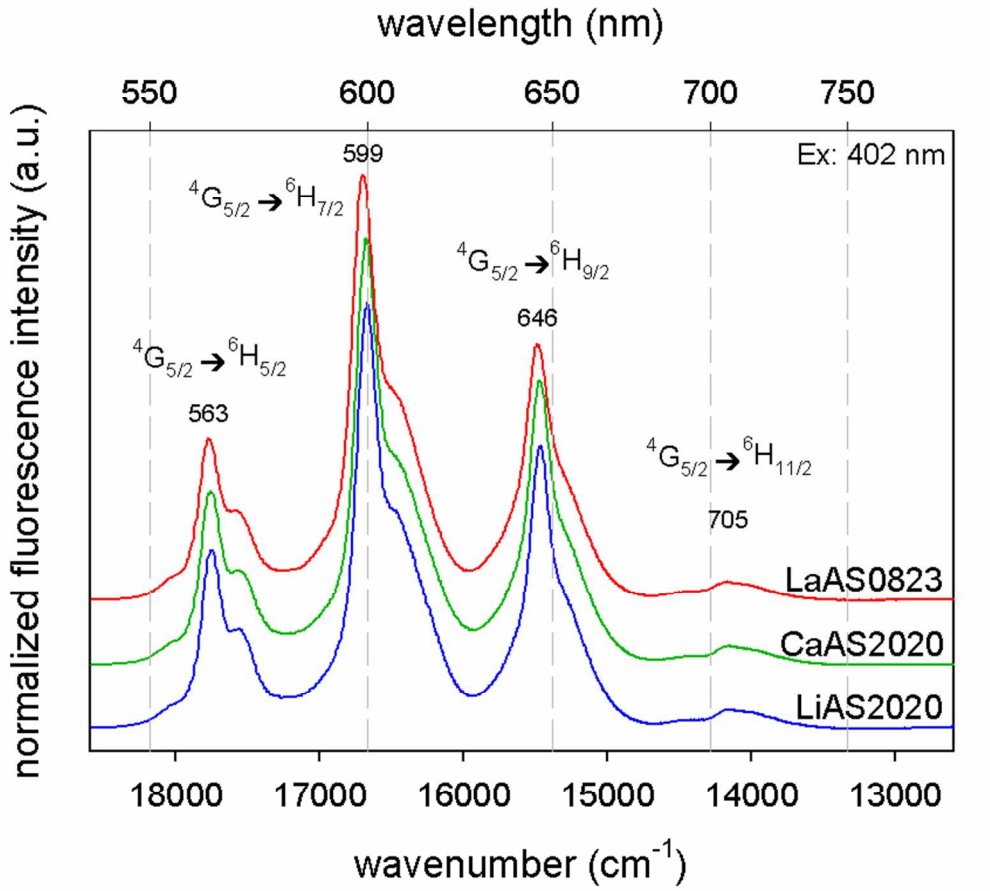

Fig. 3: Sm3+ emission spectra of samples LiAS2020, CaAS2020 and LaAS0823 doped with 1·1020 Sm3+/cm3. Note that the different spectra have been shifted in vertical direction for clarity.
144x129mm (150 x 150 DPI)

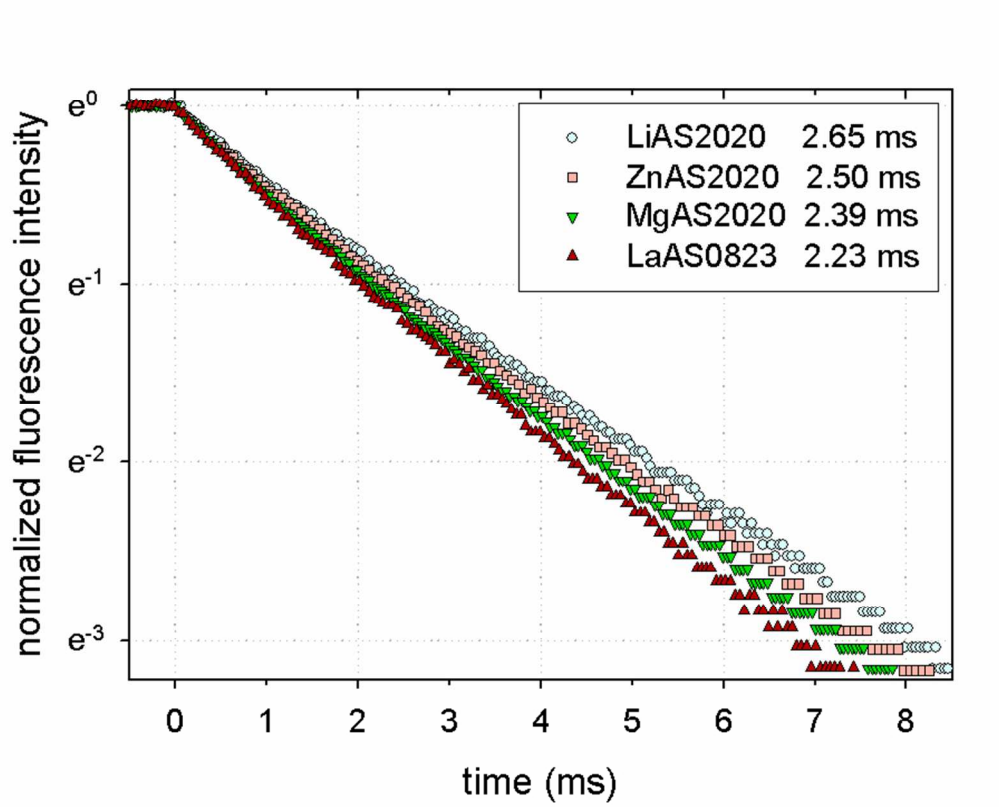

Fig. 4: Fluorescence decay curves of the 4G5/2 energy level of Sm3+ and decay times (inset) for different glass compositions.
152x123mm (150 x 150 DPI)

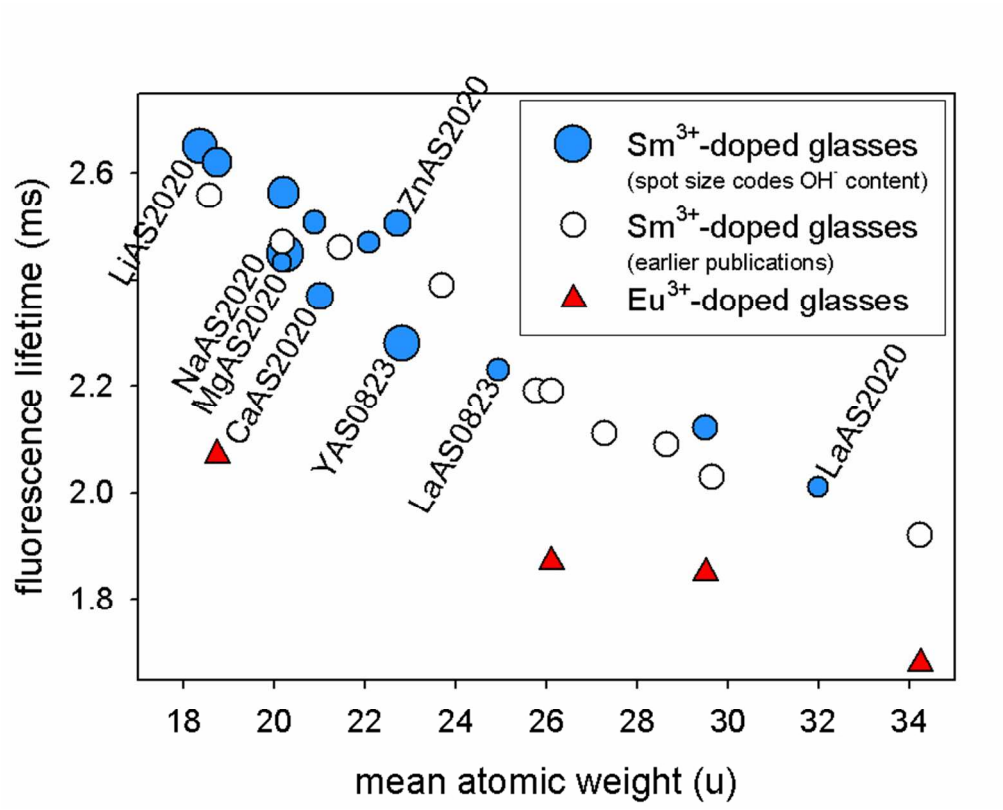

Fig. 5: Fluorescence lifetimes of ternary alumino silicate glasses doped with 1·1020 cm-3 Sm3+ (circles) and Eu3+ (triangles) in dependence of the mean atomic weight of the glass composition. The filled circles represent the Sm3+-doped samples of this publication. For these, the circle size represents the OH- concentration of the specific sample.
153x123mm (150 x 150 DPI)

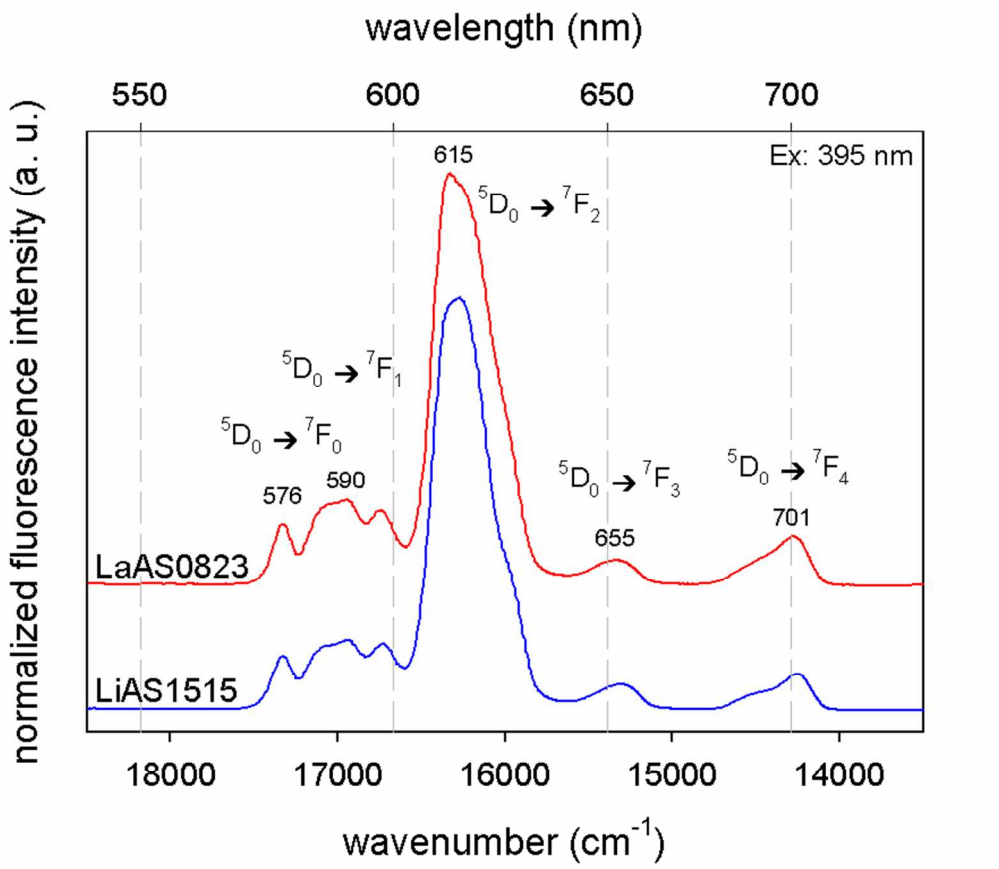

Fig. 6: Eu3+ emission spectra of a lithium (LiAS1515) and a lanthanum alumino silicate glass (LaAS0823) doped with 1·1020 Eu3+/cm3. Note that the different spectra have been shifted in vertical direction for clarity.
149x129mm (150 x 150 DPI)

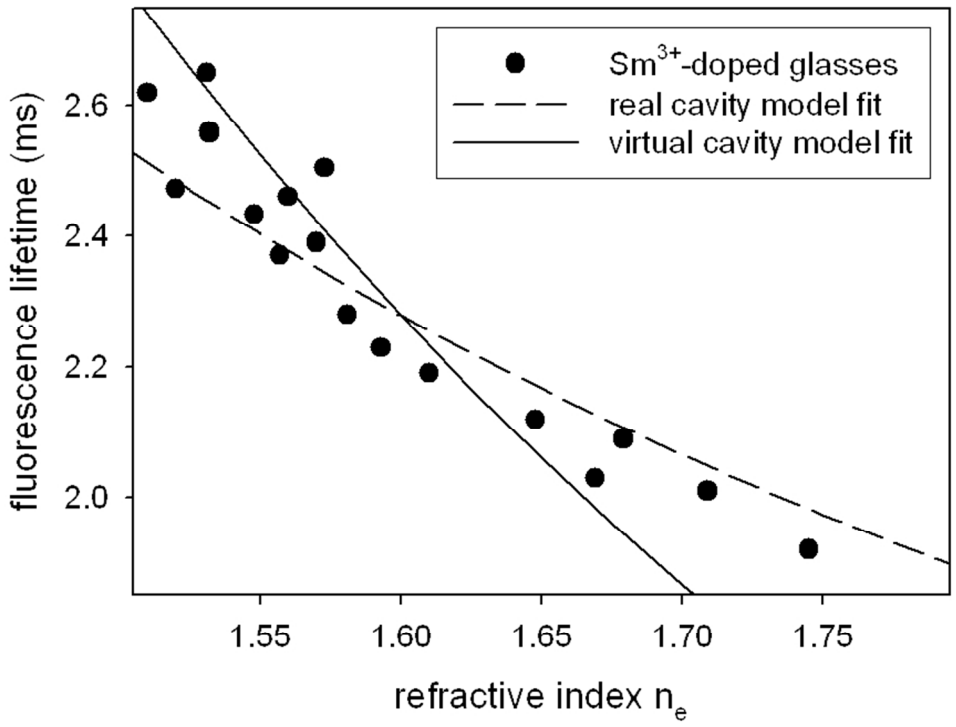

Fig. 7: Fluorescence lifetimes of ternary alumino silicate glasses doped with 1·1020 cm-3 Sm3+ in dependence of the refractive index ne of the glasses. The data has been fitted with the real and virtual cavity model.
153x124mm (150 x 150 DPI)

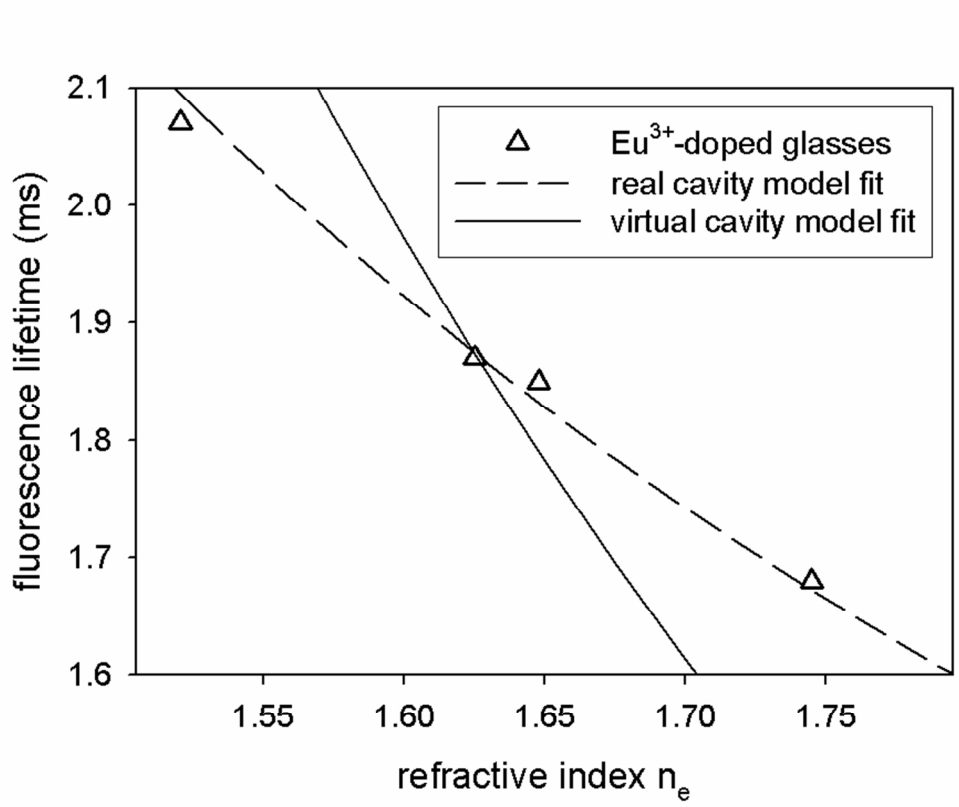

Fig. 8: Fluorescence lifetimes of ternary alumino silicate glasses doped with 1·1020 cm-3 Eu3+ in dependence of the refractive index ne of the glasses. The data has been fitted with the real and virtual cavity model.
153x124mm (150 x 150 DPI)

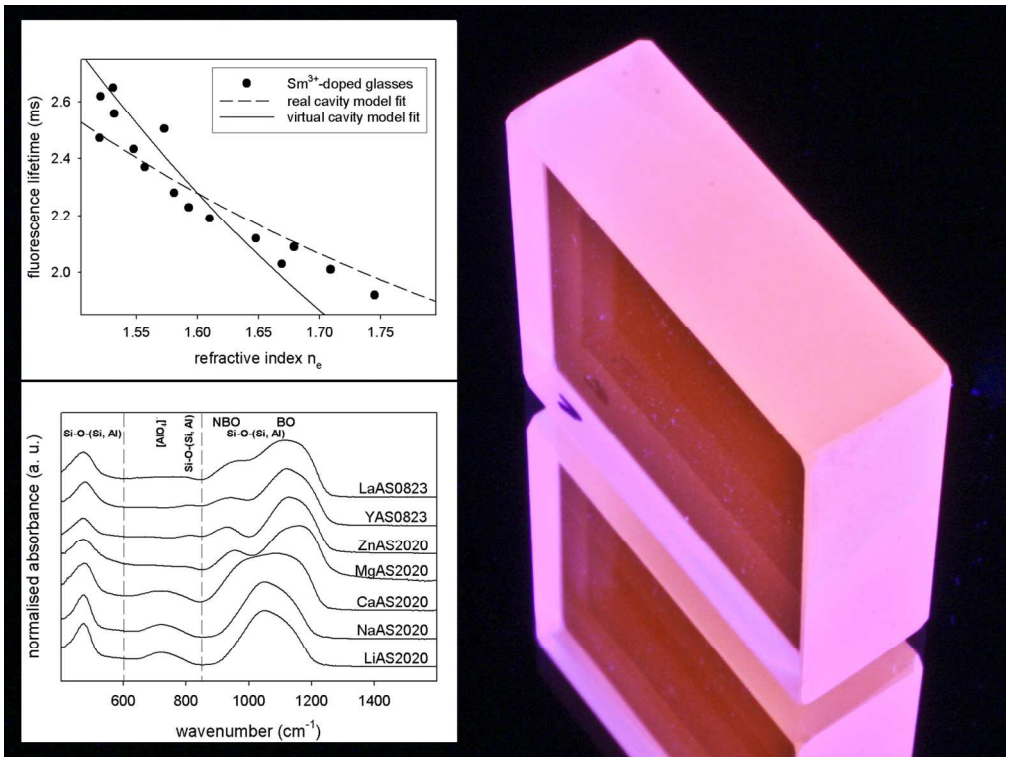

Graphical Abstract: A red fluorescent Sm3+-doped alumino silicate glass under UV excitation. The inset shows the dependence of the Sm3+ fluorescence lifetime on the refractive index of the glass (upper diagram) and the influence of the network modifying ion on the molecular structure of the glass (FTIR spectra, lower diagram).